2010 IEEE International Conference on Robotics and Automation
Anchorage Convention District
May 3-8, 2010, Anchorage, Alaska, USA

Backdrivability Analysis of Electro-Hydrostatic Actuator and Series Dissipative Actuation Model

Hiroshi Kaminaga, Tomoya Amari, Yukihiro Katayama,
Junya Ono, Yuto Shimoyama, and Yoshihiko Nakamura

Abstract— **Although backdrivability is recognized as an important property of actuators, this term is often used without clear definition. In order to design mechanisms with advanced controllability, it is important to understand the fundamental mechanism of backdrivability. In this paper, we introduced idea of series elasticity and series dissipation of actuators. Based on this idea, total / output backdrivability and their fundamental properties are stated. EHA was shown to be series dissipative and it was confirmed from the model of the actuator. Utilizing the backdrivability of EHA, position based impedance control was implemented and evaluated. Application of this EHA in a robot hand is also reported.**

I. Introduction

The term backdrivability is often ill-defined. Although it is recognized as an important functionality of actuator systems, the term is often used without clear definition of the phenomena. For an example, questions as "*What is the difference between backdrivability of gear drives pneumatic actuators?*", or "*What is the difference between backdrivability of ball screws and series elastic actuators?*" often leads to vague answer.

The property "backdrivability" is becoming increasingly important to deal with force interaction. The control systems in textbooks assume bilateral force transmission, which is not necessarily true in the real world. To overcome this problem, force based control are used as in [1] and [2]. To make design process more intuitive, force based impedance control or admittance control [3] is used in combination with high performance robots [4]. However, control relying on force measurement is often fragile when an impact was given to the system. By having backdrivability, displacement based impedance control becomes possible, which is expected to have more stable behavior even under rough conditions.

Importance of compliance in manipulation is well recognized. Winböck et al. [5] is one of the recent example of study in admittance control on robot hand. We have been studying backdrivability in motor driven displacement control type hydraulic actuator called EHA (Electro-Hydrostatic Actuator) and its application on humanoid robot [6], [7]. In

This work was supported partially by Grant-in-Aid for Scientific Research (No.20-10620) for Research Fellowships of the Japan Society for the Promotion of Science for Young Scientists and partially by "IRT Foundation to Support Man and Aging Society" under Special Coordination Funds for Promoting Science and Technology from MEXT.

H. Kaminaga, Y. Katayama, T. Amari, J. Ono, Y. Shimoyama, and Y. Nakamura are with Department of Mechano-Informatics, The University of Tokyo, 7-3-1 Hongo, Bunkyo-Ku, Tokyo 113-8656, Japan {kaminaga, katayama, amari, junya, nakamura}@ynl.t.u-tokyo.ac.jp, yuto-s@iis.u-tokyo.ac.jp

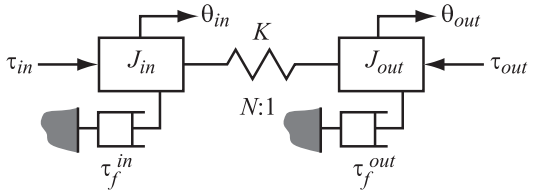

Fig. 1. Conceptual Diagram of Series Elastic Actuation

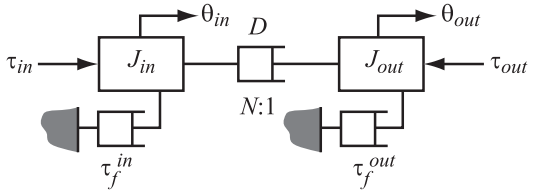

Fig. 2. Conceptual Diagram of Series Dissipative Actuation

[7], we have pointed out that there are at least two types of backdrivability that needs to be defined in order to fully describe the property of backdrivability in EHAs: total and output backdrivability.

One of the objectives of this work is to describe the backdrivability in various mechanisms and evolve design methodology for backdrivability enhancement. Another objective of this work is to understand the property of EHA as a specific case, and study the behavior in actual mechanism.

In this paper, we introduced the idea of series dissipation and series elasticity of actuators to understand the necessary difference in strategy for enhancing backdrivability according to the actuation principle. We also explained the fundamental backdrivability property of EHA and designed position based impedance controller utilizing the backdrivability. The controller was implemented and evaluated using an EHA driven robot hand.

II. Series Dissipative Actuator and Series Elastic Actuator

SEAs (Series Elastic Actuators) [8] are one type of elastic joint mechanism that was developed to enhance actuator backdrivability with non-backdrivable reducers. SEAs intentionally put spring in series to the power transmission to decouple link side dynamics from motor side dynamics. The model of SEA is essentially same with the normal elastic

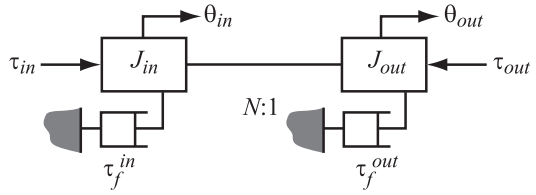

Fig. 3. Conceptual Diagram of Rigid Mechanical Actuation

joint model proposed by Spong [9] and given by (1).

$$J_{out}\ddot{\theta}_{out} + C(\dot{\theta}_{out}, \theta_{out})\dot{\theta}_{out} + K(\theta_{out} - \theta_{in}/N) = \tau_{out} - \tau_f^{out} \quad (1a)$$

$$J_{in}\ddot{\theta}_{in} - \frac{K(\theta_{out} - \theta_{in}/N)}{N} = \tau_{in} - \tau_f^{in} \quad (1b)$$

Here, θ_{in} and θ_{out} are motor and link side position respectively. τ_{in} is the motor torque and τ_{out} is the external torque from link side. τ_f^{in} and τ_f^{out} are motor and link side friction torques. C is the Coriolis force and K is the stiffness of the spring connecting the reducer output and the link. N is the reduction ratio of the transmission. SEAs are a type of actuator with position coupling between input side equation and output side equation. Conceptual diagram of SEA is shown in Fig. 1.

From (1), it is clear that the minimum output backdriving torque [7] is τ_f^{out} at $\dot{\theta}_{out} = 0$, thus the stiction torque of link side, if the deflection of the spring is zero. This is a significant reduction in minimum backdriving torque because if there is no spring decoupling the dynamics, minimum backdriving torque is $\tau_f^{out} + N\tau_f^{in}$ at $\dot{\theta}_{out} = \dot{\theta}_{in} = 0$ (See Fig. 2). Hence, when N is large, minimum backdriving torque increases significantly, deteriorating backdrivability.

Similarly, there are actuator systems with input side equation and output side equation coupled with velocity terms. EHA is an example of this class of actuator. Detailed model of EHA is described in section III. This is essentially a system coupled with damping because the transmitted force is proportional to the scaled relative velocity (See Fig. 2). We name this class of actuator a Series Dissipative Actuator or a SDA. As in the case of SEA, decoupling reduces the minimum backdriving torque significantly.

In the SDA, to decouple the dynamics of the input and output, reduction of the damping factor is necessary. Reduction in damping results in reduction of efficiency. Thus in SDAs, output backdrivability and efficiency is in trade-off relation. It should be noted that this relation is not limited to EHA, but holds for any system with series dissipative type actuator.

For the SEA, reduction of stiffness is necessary in output backdrivability enhancement, which result in reduction of resonance frequency. Thus, in SEAs, control bandwidth and output backdrivability is in trade-off relation.

Distrubuted macro mini actuation [10] is a combination of series elastic actuation and rigidly connected motor. Fig. 4 shows a single joint of distributed macro mini actuation. In [10], multiple joints are used to realize high backdrivability at low frequency and high control bandwidth simultaneously. The mini part only exerts small torque but it has high control bandwidth.

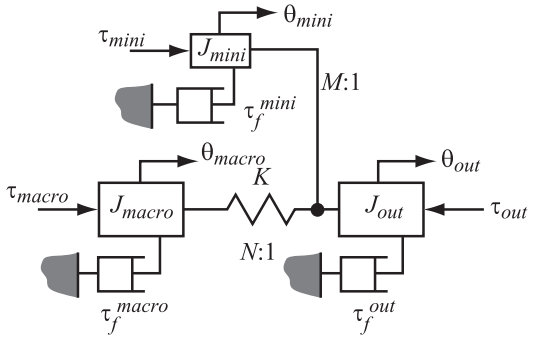

Fig. 4. Conceptual Diagram of Distributed Macro Mini Actuation

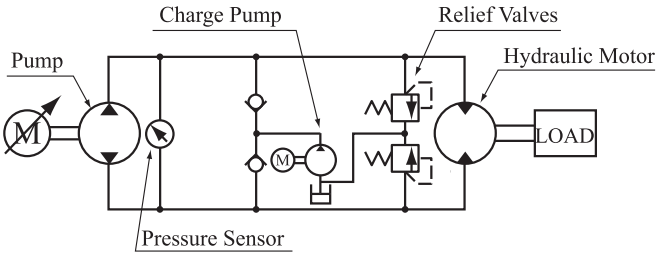

Fig. 5. Hydraulic Schematic of Electro-Hydrostatic Actuator

III. Model of Electro-Hydrostatic Actuator

EHAs are a class of servo motor driven displacement control type hydraulic system with typical architecture shown in Fig. 5. The equation of motion of an EHA is given as follows [7] [1].

$$J_i\ddot{\theta}_i = -k_3^i p_i - \tau_f^i(\dot{\theta}_i, p_i, \bar{p}) + \tau_i = -k_1^i k_3^i \dot{\theta}_i + k_2^i k_3^i \dot{\theta}_{\bar{i}} - \tau_f^i(\dot{\theta}_i, \dot{\theta}_{\bar{i}}, \bar{p}) + \tau_i \quad (2)$$

$$(i, \bar{i}) \in \{(p, m), (m, p)\} \quad (3)$$

Here, the parameters used in the equation is explained in Table I. $k_{\{1,2,3\}}^i$ are constants determined by form and hydraulic properties, such as pump thickness and hydraulic viscosity. Subscript and superscript i are either p or m. p show pump parameters and m show hydraulic motor parameters. Subscript and superscript $\bar{i}$ shows other side of i, thus if $i = p$ then $\bar{i} = m$ and Vice Versa.

Relation between pressure difference p_i and pump/hydraulic motor speed is explained as (4).

$$p_i = k_1^i \dot{\theta}_i - k_2^i \dot{\theta}_{\bar{i}} \quad (4)$$

The EHA studied in this paper uses the combination of revolute pump and revolute hydraulic motor, but any combination of prismatic and revolute applies to the formulation.

[1]The compressibility of the fluid (silicone oil) is neglected because in the pressure range we use, that is less than 10(MPa) in any case, compressibility of the fluid is less than 1% at the temperature of 25(°C) according to [11]. Even at the temperature of 100(°C), the compressibility is less than 1.5%.

TABLE I

NOMENCLATURE

Symbol	Description (units)	
	Prismatic	Revolute
θ_i	Position (m)	Angular position (m)
J_i	Mass (kg)	Moment of inertia ($\mathrm{kg \cdot m^2}$)
τ_f^i	Friction force (N)	Friction Torque (Nm)
τ_i	Input force (N)	Input torque (Nm)
p_i	Pressure difference (Pa)	
$\bar{p}$	Amount of pressurization (Pa)	

IV. Backdrivability in Electro-Hydrostatic Actuators

Since EHA is a SDA type actuator, discussion in section II implied that the dissipation term in the actuator determines the ease of backdrivability. In this section, we derive the backdriving condition from the actuator model and confirm validity of the discussion in section II.

In order to discuss the backdrivability, we need a friction model of the actuator. Friction acting on the system can be categorized to bearing friction, oil seal friction, and fluid friction. We put this as τ_{fb}^i, τ_{fs}^i, and τ_{ff}^i respectively.

$$\tau_f^i = \tau_{fb}^i + \tau_{fs}^i + \tau_{ff}^i \tag{5}$$

We made following assumptions:

1) Bearing frictions are divided into friction caused by radial and thrust bearings.
2) Normal load on bearing is given as $\max(f, f_p)$ for load f and bearing preload f_p.
3) Load on radial bearing is proportional to exerted force (torque).
4) Load on radial bearing is proportional to amount of pressurization.
5) Load on oil seal is proportional to amount of pressurization.

Assumption 4 and 5 is made because on these components, both high pressure and low pressure have effect, so they cancel out as the result.

Using the friction model proposed by Canudas De Wit [12], these friction forces (torques) can be expressed as follows.

$$\begin{aligned}\tau_{fb}^i(\dot{\theta}, p_i, \bar{p}) &= \mathrm{sgn}(\dot{\theta}_i)\left\{k_{cbr}^i + \left(k_{sbr}^i - k_{cbr}^i\right) e^{-\left(\dot{\theta}_i/\dot{\theta}_{sbr}\right)^2}\right\} \\ &\quad \times \max(|p_i|, p_{br0}^i) + k_{vbr}^i \dot{\theta}_i \\ &\quad + \mathrm{sgn}(\dot{\theta}_i)\left\{k_{cbt}^i + \left(k_{sbt}^i - k_{cbt}^i\right) e^{-\left(\dot{\theta}_i/\dot{\theta}_{sbt}\right)^2}\right\} \\ &\quad \times \max(\bar{p}, p_{bt0}^i) + k_{vbt}^i \dot{\theta}_i \end{aligned} \tag{6}$$

$$\begin{aligned}\tau_{fs}^i(\dot{\theta}_i, p_i, \bar{p}) &= \mathrm{sgn}(\dot{\theta}_i)\left\{k_{cs}^i + \left(k_{ss}^i - k_{cs}^i\right) e^{-\left(\dot{\theta}_i/\dot{\theta}_{ss}\right)^2}\right\}\left(\bar{p} + p_{s0}^i\right) \\ &\quad + k_{vs}^i \dot{\theta}_i \end{aligned} \tag{7}$$

$$\tau_{ff}^i(\dot{\theta}_i, p_i, \bar{p}) = k_{vf}^i \dot{\theta}_i \tag{8}$$

Where all k are constants. The first subscript c, s, and v are Coulomb friction, static friction, and viscous friction respectively. Second subscript b, s, and f shows bearing friction, oil seal friction, and fluid friction respectively. Third subscript r and t are radial and thrust respectively.

p_{br0}^i and p_{bt0}^i are equivalent pressure of amount of bearing preloads. p_{s0}^i is the pressure that the oil seal exerts against the shaft at vacuum. $\dot{\theta}_{s\{br,bt,s\}}$ are the speed that static friction act.

Using this friction model, output and total backdriving condition can be written as follows.

Output Backdriving Condition

$$\tau_m > k_{sbr}^m p_{br0}^m + k_{sbt}^m \max(\bar{p}, p_{bt0}^m) + k_{ss}^m \left(\bar{p} + p_{s0}^m\right) \tag{9}$$

Total Backdriving Condition

Necessary condition

$$k_3^p > k_{sbr}^p \tag{10}$$

and output backdrivability (to exert $\dot{\theta}_m$).

Sufficient Condition

If $|p_p| > p_{br0}^p$

$$\dot{\theta}_m > \frac{k_{sbt}^p \max(\bar{p}, p_{bt0}^p) + k_{ss}^p \left(\bar{p} + p_{s0}^p\right)}{k_2^p \left(k_3^p - k_{sbr}^p\right)} \tag{11a}$$

If $|p_p| \leq p_{br0}^p$

$$\dot{\theta}_m > \frac{k_{sbr}^p p_{br0}^p + k_{sbt}^p \max(\bar{p}, p_{bt0}^p) + k_{ss}^p \left(\bar{p} + p_{s0}^p\right)}{k_2^p k_3^p} \tag{11b}$$

For the total backdriving, the condition essentially relies on the speed of the hydraulic motor, but torque condition can also be derived if the driving speed of the hydraulic motor is constant. It must be noted that the necessary condition (10) must always be satisfied.

If $|p_p| > p_{br0}^p$

$$\begin{aligned}\tau_m > &\left(k_1^m k_3^m + k_{vbr}^m + k_{vbt}^m + k_{vs}^m + k_{vf}^m + k_1^m k_{cbr}^m\right) \\ &\times \frac{k_{sbt}^p \max(\bar{p}, p_{bt0}^p) + k_{ss}^p \left(\bar{p} + p_{s0}^p\right)}{k_2^p \left(k_3^p - k_{sbr}^p\right)} \\ &+ k_{cbr}^m \max(k_1^m \dot{\theta}_m, p_{br0}^m) + k_{cbt}^m \max(\bar{p}, p_{bt0}^m) \\ &+ k_{cs}^m \left(\bar{p} + p_{s0}^m\right) \end{aligned} \tag{12a}$$

If $|p_p| \leq p_{br0}^p$

$$\begin{aligned}\tau_m > &\left(k_1^m k_3^m + k_{vbr}^m + k_{vbt}^m + k_{vs}^m + k_{vf}^m + k_1^m k_{cbr}^m\right) \\ &\times \frac{k_{sbr}^p p_{br0}^p + k_{sbt}^p \max(\bar{p}, p_{bt0}^p) + k_{ss}^p \left(\bar{p} + p_{s0}^p\right)}{k_2^p k_3^p} \\ &+ k_{cbr}^m \max(k_1^m \dot{\theta}_m, p_{br0}^m) + k_{cbt}^m \max(\bar{p}, p_{bt0}^m) \\ &+ k_{cs}^m \left(\bar{p} + p_{s0}^m\right) \end{aligned} \tag{12b}$$

However, (12) cannot be solved in closed form because they rely on the amount of the preload and pressurization.

The term that may change backdrivability without changing reduction ratio is k_2^p [7]. This term have parameters regarding internal leakage. Since the energy dissipation in EHA that is not friction loss is solely internal leakage, validity of the discussion in section II was confirmed.

In this research, we developed low friction mechanism on both pump and vane motors. We use ball bearings with very small preload to minimize friction. We make following assumptions for the EHA.

1) Amount of bearing preload is negligible. Thus $p^i_{br0} = p^i_{bt0} = 0$.
2) Static and Coulomb friction in bearings are negligible. However, we included friction between trochoid gears in k^p_{sbr} and k^p_{cbr} because same relationship between friction and pressure holds. Thus $k^i_{sbr} = k^i_{cbr} \neq 0$ and $k^i_{sbt} = k^i_{cbt} = 0$.

Under this assumption, backdriving condition is simplified as follows.

Output Backdriving Condition (Simplified)

$$\tau_m > k^m_{ss}\left(\bar{p} + p^m_{s0}\right) \tag{13}$$

Total Backdriving Condition (Simplified)

$$\dot{\theta}_m > \frac{k^p_{ss}\left(\bar{p} + p^p_{s0}\right)}{k^p_2\left(k^p_3 - k^p_{sbr}\right)} \tag{14}$$

Total backdriving torque in the simplified case is given as follows.

$$\tau_m > \left(k^m_1 k^m_3 + k^m_{vs} + k^m_{vf}\right)\frac{k^p_{ss}\left(\bar{p} + p^p_{s0}\right)}{k^p_2\left(k^p_3 - k^p_{sbr}\right)} + k^m_{cs}\left(\bar{p} + p^m_{s0}\right) \tag{15}$$

V. Impedance Control in Electro-Hydrostatic Actuators

A. Inertia Scaling Control of EHA with Pressure Sensor

Traditionally, hydraulic actuators were targeted for high-output non-backdrivable application such as industrial robots and construction machines. Main objective of control in these applications were to minimize position error. Wang et al.[13] used sliding mode control on EHA to eliminate the effect of nonlinear friction. However, in this research, we wish to realize compliant behavior on EHA, thus we must design controller that can handle bi-directional operation. Typical controller is impedance control[3] that modifies dynamical behavior of the system by feedback control. Cheng et al.[14] use impedance control on whole body hydraulically driven humanoid CB, but the actuator dynamics is fundamentally different in valve controlled hydraulics and EHA. We are interested in developing impedance controller on EHA, especially the controller that measures displacement and produce force according to the displacement; which is said to be more robust against impacts.

In this research, we divide impedance control into two parts: inertia scaling on motor side dynamics and compliance control. Inertia scaling is the method to reduce apparent inertia by feedback control. This strategy is similar to the one performed by Ott et al.[15]. This is reasonable approach because force or acceleration signal quality is usually poor and thus the feedback using them should only be done in collocated control to prevent instability.

Inertia scaling in essentially a torque or acceleration feedback. However, acceleration feedback is noisy and torque sensor is often bulky. In torque sensors, stiffness of the sensor and measurement resolution are contradicting conditions. Lack of stiffness can cause coupled vibration of the system.

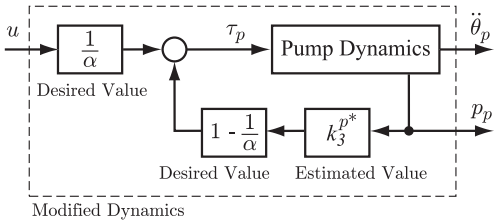

Fig. 6. Controller Structure of Inertia Scaling

We utilize the fact that in EHA, torque can be estimated from the hydraulic pressure, that can be measured by small and rigid MEMS sensors. This fact enables us to measure the torque without losing the stiffness of the system.

Using the relationship of (2) and (4), the pump side equation of motion is rewritten as follows.

$$J_p\ddot{\theta}_p = -k^p_3 p_p - \tau^p_f + \tau_p \tag{16}$$

Inertia scaling control was done by pressure feedback as in (17) to the system (16).

$$\tau_p = \frac{1}{\alpha}u + \left(1 - \frac{1}{\alpha}\right)k^{p*}_3 p_p \tag{17}$$

$$\alpha = \tilde{J}_p / J_p \tag{18}$$

Here, $\tilde{J}_p$ is the desired pump inertia, k^{p*}_3 is the estimated value of k^p_3, and u is the intermediate control input, which is used instead of τ_p. Considering the purpose of reducing the inertia, α is chosen as $0 < \alpha < 1$. See Fig. 6 for the controller structure.

It is obvious that the pressure feedback (17) modifies the dynamics of the system to (19) when $k^p_3 = k^{p*}_3$ holds.

$$\alpha J_p\ddot{\theta}_p = -k^p_1 k^p_3\dot{\theta}_p + k^p_2 k^p_3\dot{\theta}_m - \tilde{\tau}^p_f + u \tag{19}$$

Here, $\tilde{\tau^p_f} = \alpha\tau^p_f$. Thus pump friction is reduced by this feedback as well.

Let us consider the case when the parameter uncertainty exists. Consider the case when k^{p*}_3 can be written in the form of $k^{p*}_3 = (1+\epsilon)k^p_3$, with variation ϵ. Equation (19) becomes as follows with the feedback (17).

$$\frac{\alpha}{1+(1+\alpha)\epsilon}J_p\ddot{\theta}_p = -k^p_1 k^p_3\dot{\theta}_p + k^p_2 k^p_3\dot{\theta}_m - \frac{\alpha}{1+(1+\alpha)\epsilon}\tau^p_f + \frac{1}{1+(1+\alpha)\epsilon}u \tag{20}$$

This means the basic dynamics is preserved with error rate of $1 : (1+(1+\alpha)\epsilon)$. It is obvious that the natural dynamics of the original system is stable. Since modified dynamics (20) preserves the dynamics structure, modified system is also stable. Unless the upper layer controller stability is critical, it is less likely to lead to instability.

Since the output backdrivability is determined by τ^m_f, it is unchanged by this control, but total backdrivability is

enhanced with this control law with reduction of τ_f^p. Back-driving torque during acceleration is reduced by reduction of the reflected inertia.

B. Compliance Control of EHA

Compliance control realizes virtual stiffness and virtual damping by control.

We put following assumptions:

1) Inertia of the pump is sufficiently smaller than that of hydraulic motor. i.e. $\alpha J_p << J_m$
2) Reduction ratio is sufficiently larger. i.e. $\dot{\theta}_m << \dot{\theta}_p$
3) Pump friction is sufficiently small. i.e. $\alpha\tau_f^p << 1$
4) Pressure loss due to flow caused by internal leakage is sufficiently small. i.e. $k_1^i - k_2^i << 1$

Under these assumptions, system is reduced as follows when the acceleration of the system is not large.

$$\tau_m = \frac{k_3^m}{k_3^p} u + \tau_f^m \tag{21}$$

Let us put the desired spring-damper behavior of the system as follows:

$$\tau_m = D(\dot{\theta}_m^{ref} - \dot{\theta}_m) + K(\theta_m^{ref} - \theta_m) \tag{22}$$

Here, θ_m^{ref} is the reference position, $\dot{\theta}_m^{ref}$ is the reference velocity, K^{ref} is the desired stiffness, and D^{ref} is the desired damping. θ_m and $\dot{\theta}_m$ are measured (or estimated) values. [2]

To realize this behavior, compliance controller is given by (23), with k_3^{p*} and k_3^{m*} the estimated values. The compensation of τ_f^m is omitted here. It should be treated with other framework.

$$u = \frac{k_3^{p*}}{k_3^{m*}} \left\{ K(\theta_m^{ref} - \theta_m) + D^{ref}(\dot{\theta}_m^{ref} - \dot{\theta}_m) \right\} \tag{23}$$

The system dynamics with this feedback applied becomes as follows:

$$\dot{\boldsymbol{x}} = A\boldsymbol{x} - T_f + F_m\tau_m \tag{24}$$

where

$$\boldsymbol{x} = \begin{bmatrix} \dot{\theta}_p & \theta_m & \dot{\theta}_m \end{bmatrix}^T \tag{25}$$

$$\begin{aligned} &A = [a_{ij}] \\ &a_{11} = -\frac{1}{\alpha J_p} k_1^p k_3^p,\ a_{12} = -\frac{1}{\alpha J_p}\frac{k_3^{p*}}{k_3^{m*}} K^{ref} \\ &a_{13} = \frac{1}{\alpha J_p}\left(k_2^p k_3^p - \frac{k_3^{p*}}{k_3^{m*}} D^{ref} \right),\ a_{23} = 1 \\ &a_{31} = \frac{1}{J_m} k_2^m k_3^m,\ a_{33} = -\frac{1}{J_m} k_1^m k_3^m \\ &a_{21} = a_{22} = a_{32} = 0 \end{aligned} \tag{26}$$

$$T_f = \begin{bmatrix} \frac{\tau_f^p}{J_p} & 0 & \frac{\tau_f^m}{J_m} \end{bmatrix}^T \tag{27}$$

$$F_m = \begin{bmatrix} 0 & 0 & \frac{1}{J_m} \end{bmatrix}^T \tag{28}$$

[2]Since we eliminated the effect of acceleration of the hydraulic motor, (22) seems as desired mass is 0. In full system without system reduction, J_m is present, so the actual behavior includes inertia J_m.

It is difficult to perform an analytic evaluation of stability in this form. We performed the numerical evaluation of our EHA used in the robot hand presented in section VI. We also omitted friction terms for ease of analysis. For our actuator, matrix A was calculated as follows: $a_{11} = -1.5 \times 10^5$, $a_{12} = -6.1 \times 10^6(1+\delta)K$, $a_{13} = 7.4 \times 10^6 - 6.1 \times 10^6(1+\delta)D^{ref}$, $a_{23} = 1$, $a_{31} = 8.9 \times 10^4$, $a_{33} = -7.8 \times 10^6$, and $a_{21} = a_{22} = a_{32} = 0$. δ is the parameter variation. For this configuration, system is stable for $D^{ref} \leq 0$ and $0 < K^{ref} < 1.4 \times 10^8 (\mathrm{mNm/deg})$. The range of K^{ref} is sufficiently (more than 10^6 times) larger than the desired stiffness range. Obviously, system has the zero pole when $K^{ref} = 0$ because there is no force to move θ_m toward origin. Regarding the parameter uncertainty, δ only have effects on achieved stiffness and damping, that is not sensitive to the stability.

VI. Robot Hand Design

One of the goal of this work is to realize highly back-drivable robot hand utilizing backdrivability of EHA. Special attention needs to be paid for the method to transmit torque from the actuator to the finger joints not to degrade the backdrivability. We developed an EHA driven robot hand with passive low friction wire mechanism [16]. The force transmission is done by wire pulley mechanism. The mechanism is designed so that there is no sliding contact between wires and structure to prevent friction and abrasion. EHA were gathered to form a rigid cluster. This architecture enabled us to reduce number of components and volume around actuator.

Hydrostatic actuator cluster is placed in between the finger and wrist. By taking this structure, we can prevent the complicated mechanism to route wires through the 3DOF wrist. Minimization of number of DOF was necessary to place the actuator cluster in the hand. To evaluate the dexterity of the hand, we focused on feasibility of grasp pattern reproduction. We evaluated the hand design by the number of reproducible grasp patterns of Cutkosky [17].

We were motivated by the work by Brown and Asada [18] that reported only 10 independent components were necessary to reproduce daily hand movements with reasonably small error. As a result of several trials, we chose four fingers with 15 joints - 8DOF hand as in Fig. 7. Most of the grasp patterns were realized with configuration under CAD software as in Fig. 8.

VII. Experiment

A. Dexterity of the Hand

The feasibility of executing grasp patterns proposed by Cutkosky [17](See Fig. 8) was tested on the actual robot hand.

Various shapes of Styrofoam objects were prepared for the evaluation. Evaluation was done to see if the stable grasping was possible from open finger posture.

Fig. 9 shows the test results. From the test, it was confirmed that all grasp patterns in Fig. 8 not marked impossible were accomplished.

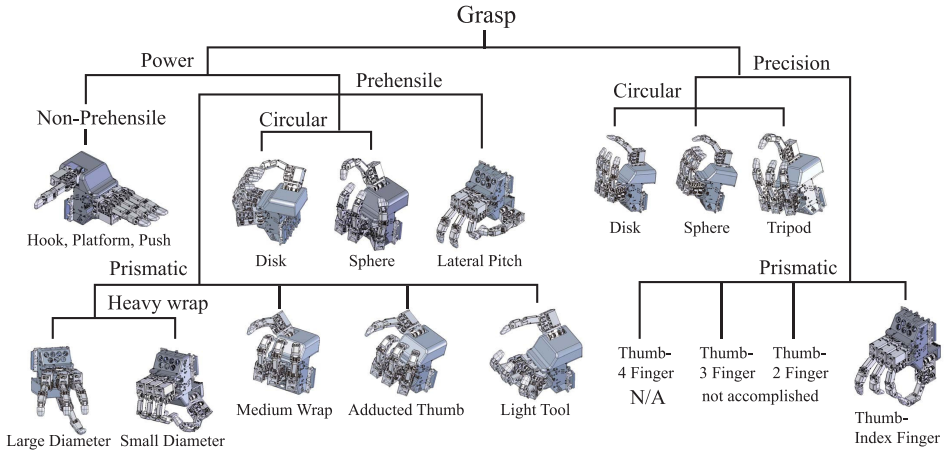

Fig. 8. Grasp Pattern Taxonomy by Cutkosky[17] Realizable with DOF of Designed Hand. Thumb-4 finger prismatic precision grasping is not available because the finger does not exist.

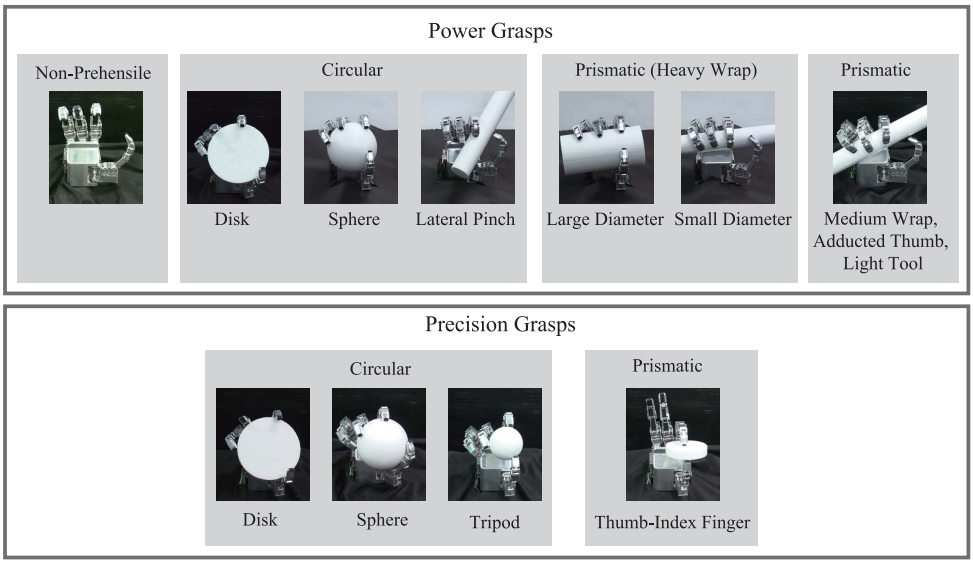

Fig. 9. Realized Grasp Patterns

B. Impedance Control

Axis level impedance control was implemented using the feedback shown in (17) and (23). The experiment was performed by applying the torque to the vane motor through a load cell while recording angular position and pressure difference at both pump and vane motor.

Two types of test was performed. In first test, fixed stiffness was selected and different amount of inertia scaling was evaluated to see the effect of inertia scaling. In the second test, fixed amount of inertia scaling was selected and different stiffness was evaluated to see the effect of compliance control.

1) Evaluation of Inertia Scaling: The stiffness of the virtual spring was set to K^{ref} =3.3(mNm/deg). Amount of inertia scaling were selected as $J_p/\tilde{J}_p$= 1, 4, 8, and 24. The damping factor D^{ref} was set to zero.

Fig. 10 shows the result. This figure shows the hysteresis loop from resting position. Dashed lines show the least square fit of the data excluding initial loop. Fig. 11 shows this repeatable portion of the hysteresis loops extracted from Fig. 10. A point that a dashed line cross y axis, hence y intercept of the dashed line corresponds to the amount of total static friction acting on EHA seen from the output axis. Table II shows the observed stiffness and friction from Fig. 10. From this table, it was confirmed that the proposed inertia scaling have no effect on stiffness, but reduces the effect of friction. Error between actual stiffness and desired stiffness was 15% when the $J_p/\tilde{J}_p = 24$. This error comes from the estimation error of k_3^{p*}.

Even the result for $J_p/\tilde{J}_p$= 24 shows some hysteresis. This hysteresis comes from friction at vane motor axis. From the relationship of applied torque to vane axis and speed of vane axis, it was confirmed that the output backdriving torque

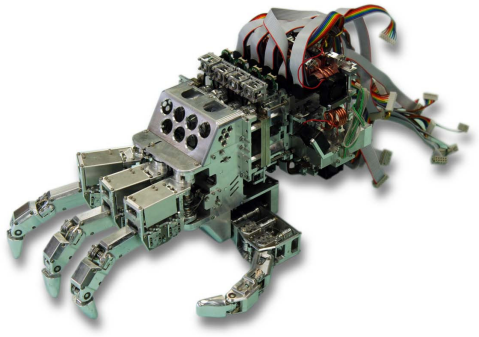

Fig. 7. Outlook of Developed Anthropomorphic Hand

TABLE II
AMOUNT OF TOTAL STATIC FRICTION AT OUTPUT AXIS OF EHA

$J_p/\tilde{J}_p$	1	4	8	24
Stiffness (mNm/deg)	2.4	2.9	3.1	2.9
Friction (mNm)	120	63	38	14

was about 20(mNm)[16]. The amount of hysteresis is about 50(mNm) for the case of $J_p/\tilde{J}_p$= 24, so the it is reasonable to think that most of the pump friction is removed by the inertia shaping.

However, the friction of vane motor cannot be measured with internal sensor of EHA. Other technique such as off-line friction identification and feed forward compensation is necessary for farther reduction of friction.

2) Evaluation of Compliance Control: The inertia scaling factor $J_p/\tilde{J}_p$ was fixed to 24 for this test. The same test method to inertia scaling evaluation was used to evaluate compliance control. Stiffness of K^{ref}=1.7, 3.3, and 6.7(mNm/deg) were tested. The damping factor D^{ref} was set to zero.

The test results are shown in Table III and Fig. 12. From

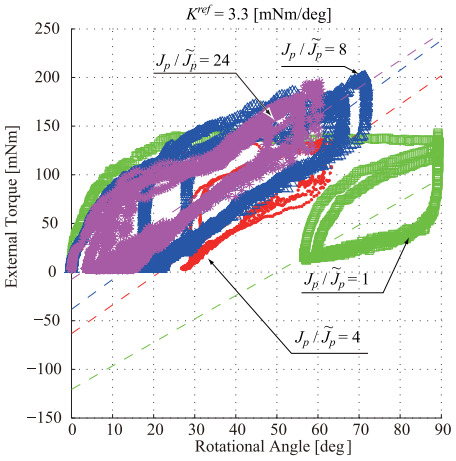

Fig. 10. Joint Impedance Control with Variable Inertia Scaling of $J_p/\tilde{J}_p = 1, 4, 8, 24$ under Fixed Desired Stiffness of 3.3(mNm/deg). Green square marker: $J_p/\tilde{J}_p = 1$, Red dot: $J_p/\tilde{J}_p = 4$, Blue triangle: $J_p/\tilde{J}_p = 8$, Magenta asterisk: $J_p/\tilde{J}_p = 24$

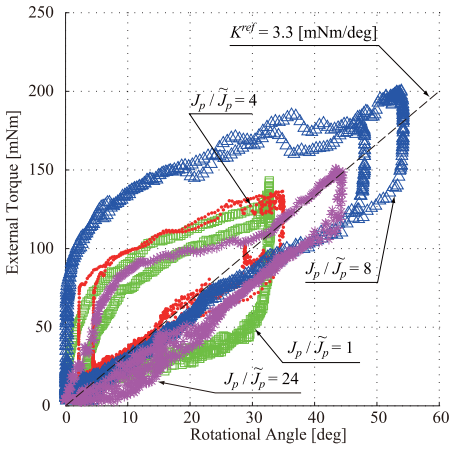

Fig. 11. Repeatable Hysteresis Loop of Joint Impedance Control with Variable Inertia Scaling of $J_p/\tilde{J}_p = 1, 4, 8, 24$ under Fixed Desired Stiffness of 3.3(mNm/deg). Makers are same as in Fig. 10.

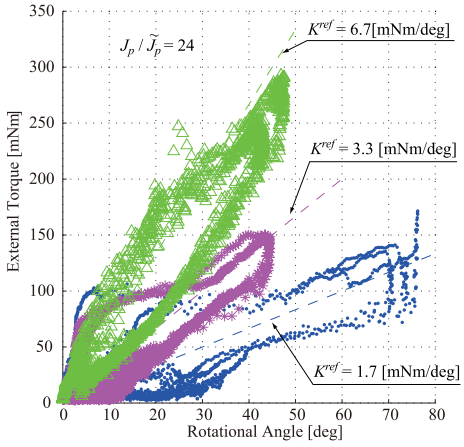

Fig. 12. Joint Impedance Control with Variable Stiffness under Fixed Inertia Scaling of $J_p/\tilde{J}_p = 24$

the result, EHA showed good stiffness realization with error of 20%. All of the traces in Fig. 12 shows hysteresis of about 50 (mNm), that is caused by vane motor friction. Also, since the error from the designed stiffness is small even for small stiffness, it was confirmed that the pump side friction is well suppressed with the inertia scaling.

Fig. 13 shows the result of grasping with impedance control enabled. A force was applied to abduction joint of the middle finger while the hand grasping spherical object. Adaptive deformation was confirmed with this experiment.

TABLE III
RESULT OF COMPLIANCE CONTROL. ALL UNITS ARE IN (mNm/deg)

Desired	1.7	3.3	6.7
Actual	1.4	2.9	5.5

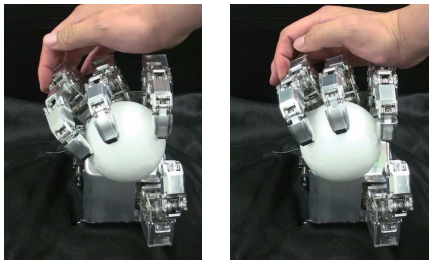

Force Released Force Applied

Fig. 13. Applying Force to Abduction Joint while Grasping Object

VIII. Conclusions

The conclusion of this paper are as follows:

1) We introduced the idea of series elasticity and series dissipation of general actuator. In either cases, decoupling of the input and output system dynamics enhances backdrivability with cost. In series elastic actuators, backdrivability and control bandwidth are trade-offs. For series dissipative actuators, efficiency and backdrivability are trade-offs. Since ideally there is no compliance in the series dissipative actuators, oscillatory behavior is less likely to happen compared to series elastic actuators. From this analysis, design strategy on backdrivability enhancement can be performed without detailed system modeling.
2) EHA was categorized as a series dissipative actuator because the system equation of pump and vane motor are connected with velocity terms. We derived quantitative properties from the proposed model of electrohydrostatic actuators. From this analysis, analysis qualitative analysis on backdrivability for series dissipative actuator was shown to be valid.
3) Strategy of impedance control was explained. Impedance control was divided into collocated inertia scaling and non-collocated compliance control. Analysis on stability of proposed controller including parameter uncertainty was made and numerically showed the stability of proposed impedance controller on designed EHA.
4) With inertia scaling control, we reduced pump inertia stably to 1/24 of the physical inertia. This significant reduction was possible due to the rigid force transmission from the motor torque to the sensor, unlike conventional torque sensing joints that use elastic elements. With reduction of the inertia to 1/24, residual friction was dominated by friction at vane motor. Thus the total backdriving torque with inertia scaling control was almost as low as output backdriving torque.
5) Impedance control showed good tracking behavior with inertia scaling even at the low virtual spring stiffness, from friction reduction effect of inertia scaling control. Stiffness was realized with the accuracy of 20%. Most of the error is expected to come from the error of parameter k_3^{i*}, which we used the design value. By identifying this parameter, we can expect enhancement in stiffness accuracy.

As a future work, we are investigating qualitative friction characteristics of oil seals using a test rig that can apply constant torque and constant speed, in different size. This test rig enables us to identify friction parameters in model of Canudas De Wit[12]. These parameters would enable us to make better estimate of the friction acting on output axis from output axis speed.

References

[1] L. E. Pfeffer, O. Khatib, and J. Hake, "Joint Torque Sensory Feedback in the Control of a PUMA Manipulator," *IEEE Trans. on Robotics and Automation*, vol. 5, no. 4, pp. 418–425, 1989.

[2] M. H. Raibert and J. J. Craig, "Hybrid Position / Force Control of Manipulators," *Trans. of ASME J. Dyn. Sys. Meas. Ctrl*, vol. 103, no. 2, pp. 126–133, 1981.

[3] N. Hogan, "Impedance Control: An Approach to Manipulation: Part I-III," *Trans. of ASME J. Dyn. Sys. Meas. Ctrl*, vol. 107, no. 1, pp. 1–23, 1985.

[4] A. Albu-Shäffer, C. Ott, and G. Hirzinger, "A Unified Passivity-based Control Framework for Position, Torque and Impedance Control of Flexible Joint Robots," *The Int'l J. of Robotics Research*, vol. 26, no. 1, pp. 23–39, 2007.

[5] T. Wimböck, C. Ott, and G. Hirzinger, "Analysis and Experimental Evaluation of the Intrinsically Passive Controller (IPC) for Multifingered Hands," in *Proc. of IEEE Int'l Conf. on Robotics and Automation*, 2008, pp. 278–284.

[6] H. Kaminaga, T. Yamamoto, J. Ono, and Y. Nakamura, "Anthropomorphic Robot Hand With Hydrostatic Actuators," in *Proc. of 7th IEEE-RAS Int'l Conf. on Humanoid Robots*, 2007, pp. 36–41.

[7] H. Kaminaga, J. Ono, Y. Nakashima, and Y. Nakamura, "Development of Backdrivable Hydraulic Joint Mechanism for Knee Joint of Humanoid Robots," in *Proc. of Int'l Conf. of Robotics and Automations*, 2009, pp. 1577–1582.

[8] G. A. Pratt and M. M. Williamson, "Series Elastic Actuators," in *Proc. of IEEE/RSJ Int'l Conf. on Intelligent Robots and Systems*, vol. 1, 1995, pp. 399–406.

[9] M. Spong, "Modeling and Control of Elastic Joint Robots," *Trans. of ASME J. Dyn. Sys. Meas. Ctrl*, vol. 109, no. 4, pp. 310–319, 1987.

[10] M. Zinn, O. Khatib, B. Roth, and J. K. Salisbury, "A New Actuation Approach for Human Friendly Robot Design," in *Experimental Robotics VIII*, ser. Springer Tracts in Advanced Robotics, B. Siciliano and P. Dario, Eds. Springer-Verlag, 2002.

[11] Shin-Estu Silicones, *The Uniquie Properties of Silicone*, web page. `http://www.silicone.jp/e/products/type/oil/detail/about/index2.shtml`.

[12] C. Canudas, H. Olsson, K. J. Åström, and P. Lischinsky, "A New Model for Control of Systems With Friction," *IEEE Trans. on Automatic Control*, vol. 40, no. 3, pp. 419–425, 1995.

[13] S. Wang, S. Habibi, R. Burton, and E. Sampson, "Sliding Mode Control for a Model of an Electrohydraulic Actuator System with Discontinuous Nonlinear Friction," in *Proc. of American Ctrl. Conf.*, 2006, pp. 5897–5904.

[14] G. Cheng, S. H. Hyon, J. Morimoto, A. Ude, G. Colvin, W. Scroggin, and S. C. Jacobsen, "CB: A Humanoid Research Platform for Exploring NeuroScience," in *Proc. of 6th IEEE-RAS Int'l Conf. on Humanoid Robots*, 2006, pp. 182–187.

[15] C. Ott, A. Albu-Schäffer, and G. Hirzinger, "A passivity based cartesian impedance controller for flexible joint robots.part i:torque feedback and gravity compensation," in *Proc. of IEEE Int'l Conf. on Robotics and Automation*, 2004, pp. 2659–2665.

[16] H. Kaminaga, J. Ono, Y. Shimoyama, T. Amari, Y. Katayama, and Y. Nakamura, "Anthropomorphic Robot Hand with Hydrostatic Cluster Actuator and Detachable Passive Wire Mechanism," in *Proc. of 9th IEEE-RAS Int'l Conf. on Humanoid Robots*, 2009, pp. 1–6.

[17] M. R. Cutkosky, "Grasp Choice, Grasp Models,and the Design of Hands for Manufacturing Tasks," *IEEE Trans. on Robotics and Automations*, vol. 5, no. 3, pp. 269–279, 1989.

[18] C. Y. Brown and H. Asada, "Inter-Finger Coordination and Postual Synergies in Robot Hands via Mechanical Implementation of Principal Component Analysis," in *Proc. of IEEE/RSJ Int'l Conf. on Intelligent Robots and Systems*, 2007, pp. 2877–2882.